Online ISSN 1848-3380, Print ISSN 0005-1144
ATKAFF 54(1), 103–113(2013)

Kenta Maeda, Hiroshi Fujimoto, Yoichi Hori

Four-wheel Driving-force Distribution Method for Instantaneous or Split Slippery Roads for Electric Vehicle

DOI 10.7305/automatika.54-1.312
UDK 681.532.6-83; 629.3.017.2
IFAC 3.2; 5.7.1

Original scientific paper

In this paper, a four-wheel driving force distribution method based on driving force control is proposed. Driving force control is an anti-slip control method, previously proposed by the authors' research group, which generates appropriate driving force based on the acceleration pedal. However, this control method cannot completely prevent reduction of driving force when a vehicle runs on an extremely slippery road. If the length of a slippery surface is shorter than the vehicle's wheel base, the total driving force is retained by distributing the shortage of driving force to the wheels that still have traction. On the other hand, when either the left or right side runs on a slippery surface, yaw-moment is suppressed by setting total driving forces of left and right wheels to be the same. Therefore, four-wheel driving force distribution method is proposed for retaining driving force on instantaneous slippery roads, and suppressing yaw-moment on split ones. The effectiveness of the proposed distribution method is verified by simulations and experiments.

Key words: Electric vehicle, Traction control, Slip ratio, Driving force, Least squares method

Metoda za raspodjelu pogonske sile električnih vozila sa četiri kotača na kratkotrajno ili polovično skliskim cestama. U ovom radu predložena je metoda za raspodjelu pogonske sile električnih vozila sa četiri kotača temeljena na upravljanju pogonskom silom. Upravljanje pogonskom silom je metoda upravljanja koju je ranije predložila autorova istraživačka grupa, a koristi se za sprječavanje proklizavanja. Ova metoda generira prikladnu pogonsku silu temeljem pritiska na papučicu ubrzanja. Ipak, ova metoda upravljanja ne može u potpunosti spriječiti smanjenje pogonske sile kada vozilo naiđe na ekstremno sklisku cestu. Ako je dužina skliske površine kraća od međuosovinskog razmaka vozila, ukupna pogonska sila se zadržava redistribucijom manjka pogonske sile na kotače koji i dalje imaju trakciju. S druge strane, kada lijeva ili desna strana vozila naiđe na sklisku površinu, moment zakretanja se potiskuje postavljanjem ukupne pogonske sile lijevih i desnih kotača na jednaki iznos. Dakle, metoda za raspodjelu pogonske sile predložena je za zadržavanje pogonske sile na kratkotrajno skliskim cestama, te za sprječavanje momenta zakretanja na polovično skliskim cestama. Učinkovitost predložene metode verificirana je simulacijski i eksperimentalno.

Ključne riječi: električno vozilo, upravljanje proklizavanjem, omjer proklizavanja, pogonska sila, metoda najmanjih kvadrata

1 INTRODUCTION

As a solution for energy and environmental problems, electric vehicles (EVs) have been receiving great attention. In addition, EVs have many advantages over internal combustion engine vehicles, since electric motors and inverters are utilized in EV drive systems. Their advantages can be summarized as follows [1]:

1. The torque response of electric motors is 10–100 times faster than that of engines.
2. All wheels can be controlled independently by adopting small high-power in-wheel motors.
3. The output torque of an electric motor can be measured accurately from the motor current.

Based on these advantages, many traction control methods for anti-skid on slippery surface have been proposed. These methods are based on torque observer [2, 3], maximum transmissible torque estimation [4], slip ratio control [5, 6], sliding mode control [7] and so on. In addition, since the road friction coefficient μ decides the maximum torque that a wheel can generate on the surface, estimation methods of the μ have been proposed [8–10].

The authors' research group also has proposed traction control methods [11–14]. Driving force control (DFC) [11], the latest one, is a control method that directly controls driving force with driving force outer loop based on driving force observer, and wheel-speed inner loop based on slip ratio control [12, 13], which can generate large yet uncertain driving force on slippery roads. With this control system, the desired driving force is generated within the saturator limits, and traction is retained by slip ratio control when the driving force saturates. Moreover, driving force commanded by a driver can be generated by using the acceleration pedal as the driving force reference.

Since DFC proposed in [11] is considered for front-wheel-driven EVs, it is inevitable that total driving force diminishes on extremely slippery roads, which also applies to the other traction control methods. However, sudden decrease of driving force leads to driver discomfort, and thus a novel control method is needed to retain total driving force. In addition, the left and right driving forces need to be equal to prevent yawing.

In this paper, a four-wheel driving force distribution method based on DFC is proposed for EV with in-wheel motors. As mentioned, it is one of EVs' advantages that all-wheel-drive vehicles can easily be realized by adopting small high-power in-wheel motors. Even when a vehicle runs into a slippery road such as scattered snow or wet manholes, whose length is shorter than the vehicle's wheel base, total driving force is retained by distributing the shortage of driving force to wheels that still have traction. Additionally, when either left or right side are on a slippery surface, yaw motion is suppressed by generating the difference between left and right driving force to follow desired yaw-moment — zero when running straight. The four-wheel driving force distribution method proposed in this paper can realize both functions simultaneously. The effectiveness of the proposed method is verified by simulations and experiments.

2 EXPERIMENTAL VEHICLE AND VEHICLE MODEL

2.1 Experimental Vehicle

The experimental EV "FPEV2-Kanon," developed by the authors' laboratory, is used for performance verification as shown in Fig. 1. In this section the characteristics of the experimental vehicle are explained.

Outer-rotor-type in-wheel motors shown in Fig. 2 are installed in each wheel. Since these motors adopt direct drive system, reaction forces from the road are directly transferred to the motors without gear reduction or backlash. The maximum torque of each of the front motors is ± 500 [Nm], and that of the rear is ± 340 [Nm]. Additionally, an optical sensor is installed to measure the vehicle velocity accurately. The vehicle's specification is expressed in Table 1.

Fig. 1. FPEV2-Kanon.

Fig. 2. In-wheel motor.

Table 1. Vehicle specifications.

Vehicle Mass (m)	870 [kg]
Wheel Base (l)	1.7 [m]
Distance from C.G to Front Axle (l_f)	0.999 [m]
Distance from C.G to Rear Axle (l_r)	0.701 [m]
Tread Base (d_f, d_r)	1.3 [m]
Wheel Radius (r)	0.302 [m]

2.2 Equations of Vehicle Dynamics

In this section, equations of vehicle dynamics are explained [11].

The equation of rotational motion of each wheel (as shown in Fig. 3) can be described as

$$J_{ij}\dot{\omega}_{ij} = T_{ij} - rF_{dij}, \tag{1}$$

where J is the wheel inertia, ω is the wheel angular velocity, T is the motor torque, r is the wheel radius, F_d is the driving force at the point where the wheel makes contact with the ground. Also, i and j are indices for f/r (front/rear) and l/r (left/right) respectively.

The equation of longitudinal motion of the vehicle body (as shown in Fig. 4) can be described as

$$m\dot{V} = F_{dfl} + F_{dfr} + F_{drl} + F_{drr}, \tag{2}$$

where m is the vehicle mass, V is the vehicle velocity.

When the vehicle accelerates or decelerates, the wheel velocity $V_\omega = r\omega$ differs from the vehicle velocity V because of tire's elastic deformation. Therefore the slip ratio λ is defined as

$$\lambda = \frac{V_\omega - V}{\max(V_\omega, V, \epsilon)}, \tag{3}$$

where ϵ is a tiny value to prevent division by zero. The driving force F_d and the driving stiffness D_s at each wheel

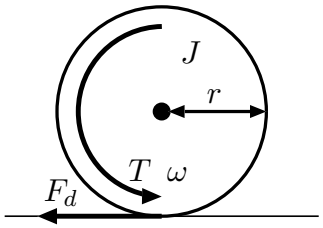

Fig. 3. Rotational motion of wheel.

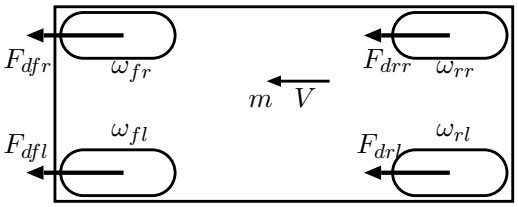

Fig. 4. Variables in vehicle motion.

are obtained as

$$F_{dij} = \mu_{ij} N_{ij}, \tag{4}$$

$$D_{sij} = \left.\frac{dF_{dij}}{d\lambda_{ij}}\right|_{\lambda_{ij}=0}, \tag{5}$$

where N is the normal reaction force on each wheel, and μ is the friction coefficient.

Figure 5 demonstrates the μ — λ relationship which depends on the road condition [15]. There are $\lambda_{\mathrm{peak,p}}$, $\lambda_{\mathrm{peak,n}}$ on which μ is the maximum or the minimum. In the domain of $\lambda_{\mathrm{peak,n}} \le \lambda \le \lambda_{\mathrm{peak,p}}$, μ is a monotonically increasing function of λ, and outside the domain, a monotonically decreasing function.

3 TRACTION CONTROL

3.1 Driving Force Control

In this section, the driving force control (DFC) method is explained [11]. The block diagram of DFC is shown in Fig. 6. The outer loop is a driving force loop based on driving force observer and the inner loop is a wheel velocity loop that controls the slip ratio. F_d^* is the driving force reference and $\hat{F}_d$ is the estimated driving force.

Since the definition of slip ratio λ for acceleration ($V_\omega \ge V$) differs from that of the definition for deceleration ($V_\omega < V$), λ is inconvenient to control. Therefore, instead of the slip ratio, the control input y, defined as follows, is controlled.

$$y = \frac{V_\omega}{V} - 1 \tag{6}$$

This is the same definition as the definition of slip ratio for deceleration. The relationship between λ and y in the domain of $\lambda > 0$ is calculated as

$$y = \frac{\lambda}{1-\lambda}, \tag{7}$$

which indicates that y equals to λ when $|\lambda| \ll 1$ and they are always one to one correspondence as shown in Fig. 7.

From (6), the wheel velocity reference V_ω^* of the inner loop is calculated as

$$V_\omega^* = (1+y)V, \tag{8}$$

which shows that the vehicle can not start moving when at rest ($V = 0$) since V_ω^* is equal to 0 independent of y. To prevent this problem, the reference V_ω^* is modified where V is smaller than a given constant σ as shown in (9).

$$\begin{cases} V_\omega^* = V + y\sigma & (V < \sigma) \\ V_\omega^* = V + yV & (V \ge \sigma) \end{cases} \tag{9}$$

From (5), it can be considered that $F_d = D_s\lambda$ provided that $|\lambda| \ll 1$. In addition, assuming that wheel velocity control is fast enough such that $y \simeq \lambda$, the transfer function from y to F_d is assumed to be zero order as

$$F_d = D_s\lambda \simeq D_s y. \tag{10}$$

Therefore, the driving force controller is set as I control with gain K_I, whose initial value is set as $y_0 = 0$. Saturation is applied to the integrator output for limiting y to $y_{\min} \le y \le y_{\max}$. With this saturation, traction can be retained by keeping the slip ratio within the domain where μ is monotonic function of λ.

In Fig. 6, feed-forward to motor torque reference T^* is obtained by adding rF_d^*, which is added anew in this paper in order to improve response speed. If the wheel has traction, then $T_{ij} \simeq rF_{dij}$ holds, since $J_{ij}\dot{\omega}_{ij}$ is assumed to be small in (1). Therefore, due to the feed-forward, the system can generate approximate driving force, and slight differences are compensated for by the driving force feedback. Also, when a wheel is on a slippery surface, traction is maintained due to the wheel-speed feed-back.

3.2 Driving Force Observer

In this section, the driving force observer (DFO) is explained.

J and r are given in (1), and ω can be measured. Moreover, the motor torque T can be controlled accurately. Therefore, with the DFO shown in Fig. 8, the driving force F_d at each wheel can be estimated with motor torque reference T^* and wheel velocity ω, assuming that current control of motor is fast enough for $T = T^*$ to be valid. τ is the time constant of the DFO.

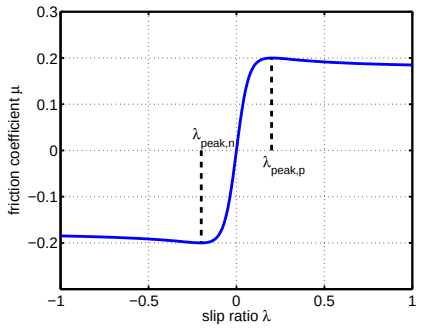

Fig. 5. Typical μ-λ relationship.

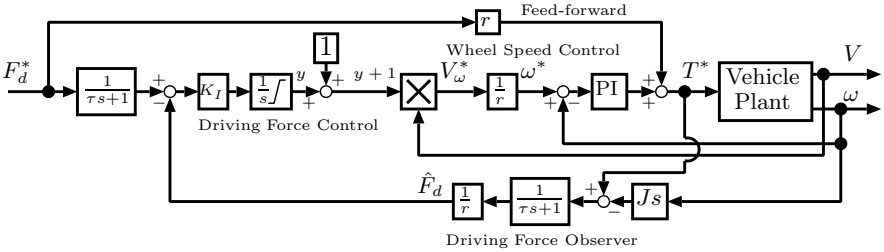

Fig. 6. Block diagram of DFC.

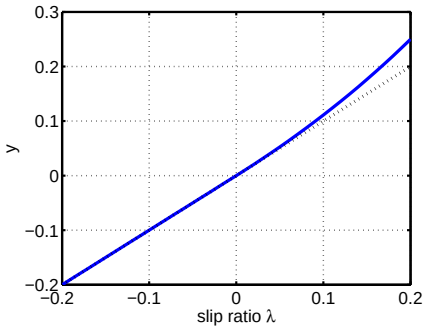

Fig. 7. The relationship between λ and y.

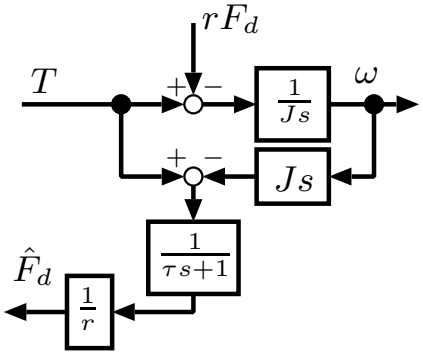

Fig. 8. Block diagram of driving force observer.

4 PROPOSED METHOD

4.1 Driving Force Distribution Method

In this section, four-wheel driving force distribution is explained. When slip ratio λ increases on a slippery surface and the control input y of DFC approaches the upper limit, driving force is saturated and reduced. To avoid this reduction, λ of each wheel need to be small enough to prevent saturation. Therefore, the proposed method decides the driving force reference F^*_{dij} of each wheel to minimize λ_{ij} of each wheel, satisfying total driving force reference F^*_{dall} and yaw-moment reference M^*_z generated by driving force difference between left and right.

The relationship between driving force of each wheel F_{dij} and F_{dall}, M_z is as follows:

$$\begin{bmatrix} 1 & 1 & 1 & 1 \\ -\frac{d_f}{2} & \frac{d_f}{2} & -\frac{d_r}{2} & \frac{d_r}{2} \end{bmatrix} \begin{bmatrix} F_{dfl} \\ F_{dfr} \\ F_{drl} \\ F_{drr} \end{bmatrix} = \begin{bmatrix} F_{dall} \\ M_z \end{bmatrix}. \tag{11}$$

Here, by setting the coefficient matrix in the left-hand side as $\boldsymbol{A}$, the vector of driving force of each wheel $[F_{dfl}, F_{dfr}, F_{drl}, F_{drr}]^T$ as $\boldsymbol{x}$, and that of total driving force and yaw-moment $[F_{dall}, M_z]^T$ as $\boldsymbol{b}$, (11) can be rewritten as $\boldsymbol{Ax} = \boldsymbol{b}$. From (10) driving stiffness of each wheel D_{sij} in the domain of $|\lambda| \ll 1$ can be obtained as

$$D_{sij} = \frac{F_{dij}}{\lambda_{ij}}. \tag{12}$$

Then the cost function J is defined as the sum of squares of slip ratio λ_{ij}.

$$\begin{aligned} J &= \lambda_{fl}^2 + \lambda_{fr}^2 + \lambda_{rl}^2 + \lambda_{rr}^2 \\ &= \frac{F_{dfl}^2}{D_{sfl}^2} + \frac{F_{dfr}^2}{D_{sfr}^2} + \frac{F_{drl}^2}{D_{srl}^2} + \frac{F_{drr}^2}{D_{srr}^2} \end{aligned} \tag{13}$$

Therefore, the weighted least squares solution $\boldsymbol{x_{opt}}$ of (11) that minimizes J, and weighting matrix $\boldsymbol{W}$ are as follows.

$$\boldsymbol{x_{opt}} = \boldsymbol{W}^{-1}\boldsymbol{A}^T(\boldsymbol{A}\boldsymbol{W}^{-1}\boldsymbol{A}^T)^{-1}\boldsymbol{b} \tag{14}$$

$$\boldsymbol{W} = \mathrm{diag}\left(\frac{1}{D_{sfl}^2}, \frac{1}{D_{sfr}^2}, \frac{\phi_r}{D_{srl}^2}, \frac{\phi_r}{D_{srr}^2}\right) \tag{15}$$

Here, ϕ_r is the tuning gain which adjust front and rear driving force distribution ratio. Larger amount of driving force

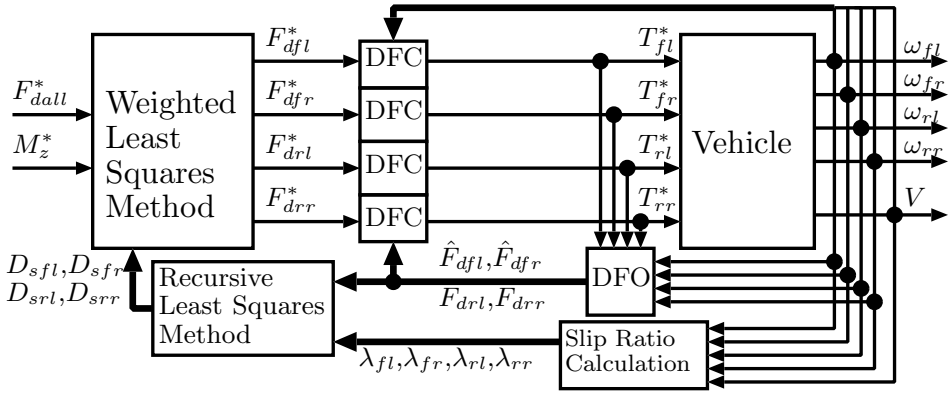

Fig. 9. Block diagram of the proposed method.

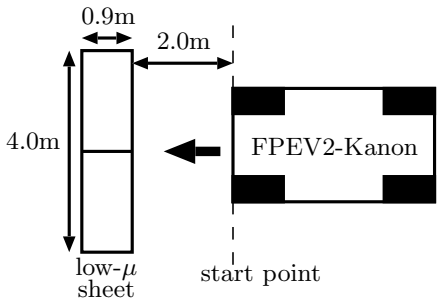

Fig. 10. Instantaneous low-μ road.

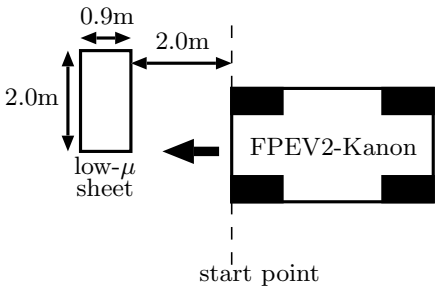

Fig. 11. Split low-μ road.

is distributed to rear wheels than front ones during acceleration, which possibly leads to excessive driving force references on rear wheels over the upper limit of rear motor torque and total driving force saturates even on a high-μ surface. Therefore ϕ_r is set as $\phi_r \geq 1$ during acceleration to prevent the saturation.

4.2 Driving Stiffness Estimation

From (12), the relationship between F_d and λ is $F_d = D_s\lambda$. Therefore the driving stiffness of each wheel at sample k $D_{sij}(k)$ can be estimated by the Recursive Least Squares (RLS) Method as follows [14].

$$\hat{D}_{sij}(k) = \hat{D}_{sij}(k-1) - \frac{\Gamma(k-1)\lambda(k)}{w + \lambda_{ij}(k)\Gamma(k-1)\lambda_{ij}(k)} \times \left[\lambda_{ij}(k)\hat{D}_{sij}(k-1) - \hat{F}_{dij}(k)\right] \quad (16)$$

$$\Gamma(k) = \frac{1}{w}\left[\Gamma(k-1) - \frac{\Gamma(k-1)\lambda_{ij}(k)^2\Gamma(k-1)}{w + \lambda_{ij}(k)\Gamma(k-1)\lambda_{ij}(k)}\right] \quad (17)$$

where w is the forgetting factor. If regressor $\lambda_{ij}(k)$ equals zero, the persistent excitation is not satisfied. Therefore $\hat{D}_{sij}(k)$ and $\Gamma(k)$ are not updated if $|\lambda_{ij}(k)| < 0.005$. Lower limitations 1000 are imposed to $\hat{D}_{sij}$ avoiding division by zero in (15).

Figure 9 shows the block diagram of the whole system. The driving force references F^*_{dij} are given by $\boldsymbol{x_{opt}}$.

5 SIMULATION

5.1 Simulation Setup

In this section, simulation results of acceleration test are explained. In this paper, “2D-Tire Model” [16] is used for vehicle running simulation.

As shown in Fig. 10 and Fig. 11, an extremely low μ ($\mu = 0.15$) surface of length 0.9 [m], shorter than the wheel base of “FPEV2-Kanon", is set at the distance of 2.0 [m] from the start point. The experimental vehicle starts at the start point and accelerates with total driving force reference $F^*_{dall} = 2000$ [N].

The parameters are, $K_I = 0.01$, $\tau = 30$ [ms], $y_{\max} = 0.25$ which corresponds to a slip ratio of $\lambda = 0.2$, $\sigma = 0.5$ [m/s]. The wheel speed PI controller is designed by the pole assignment method towards the plant $\frac{1}{Js}$, which

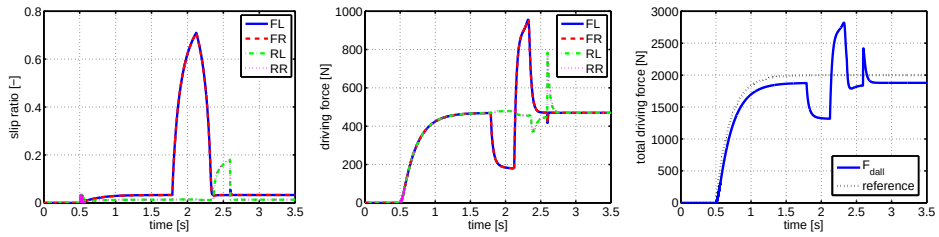

(a) λ on each wheel. (b) $\hat{F}_d$ on each wheel. (c) $\hat{F}_{dall}$.

Fig. 12. Simulation of instantaneous slippery road (without control).

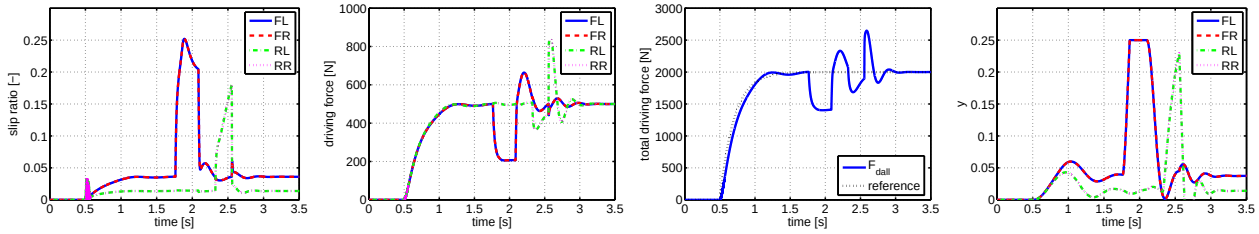

(a) λ on each wheel. (b) $\hat{F}_d$ on each wheel. (c) $\hat{F}_{dall}$. (d) y on each wheel.

Fig. 13. Simulation of instantaneous slippery road (only DFC).

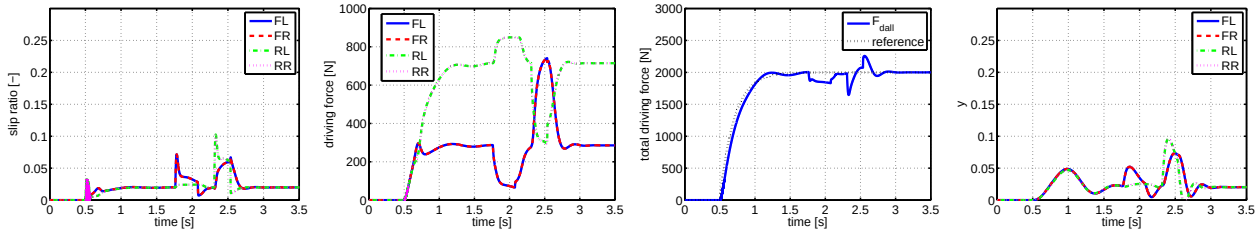

(a) λ on each wheel. (b) $\hat{F}_d$ on each wheel. (c) $\hat{F}_{dall}$. (d) y on each wheel.

Fig. 14. Simulation of instantaneous slippery road (proposed).

is from (1) ignoring F_d, setting the pole -20 [rad/s]. The forgetting factor of the driving stiffness estimation is $w = 0.995$. All parameters are the same for each wheel.

5.2 Instantaneous Slippery Road

Figures 12 – 14 show the simulation results of acceleration test on instantaneous slippery surface. In each result, front wheels are on slippery surface from about 1.8 [s] to 2.1 [s], and rear ones are from about 2.3 [s] to 2.5 [s].

The simulation results are compared with three conditions. Figure 12 shows the results of acceleration test without any traction control, i.e., motor torque on each wheel is set as $500r = 151$ [Nm] constantly. Then Fig. 13 shows the results of the conventional method with only DFC and without driving force distribution, i.e., driving force references on each wheel are the same. Finally Fig. 14 shows the results of the proposed method with DFC and the driving-force distribution.

In case without control, extreme slip occurs in Fig. 12(a) then the driving force decreases in Fig. 12(b), 12(c). In case with only DFC, although the traction is obtained in Fig. 13(a), the driving force decreases in Fig. 13(b), 13(c), similar to the case without control.

On the contrary, with the proposed method, Fig. 14(b) shows that the driving force on each wheel is distributed to retain total driving force as shown in Fig. 14(c), as well as the traction shown in Fig. 14(a). In addition, compared to Fig. 13(d), Fig. 14(d) shows that the proposed method prevents the satulation of the DFC control input y.

In Fig. 14(c), the total driving force is not completely retained and slightly decreases from the reference when front wheels are on the slippery surface. This is because

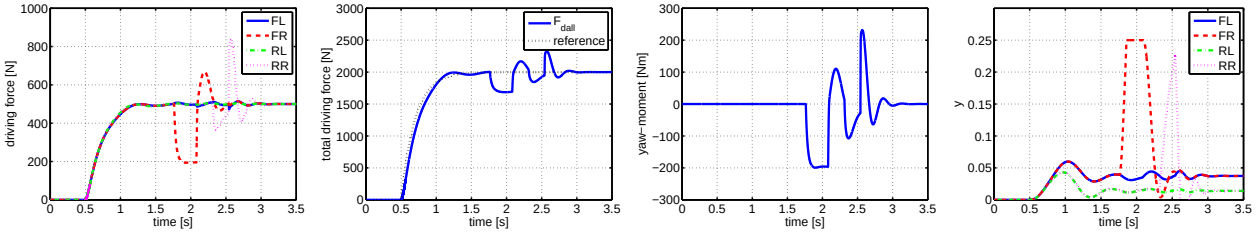

(a) $\hat{F}_d$ on each wheel. (b) $\hat{F}_{dall}$. (c) $\hat{M}_z$. (d) y on each wheel.

Fig. 15. Simulation of split slippery road (only DFC).

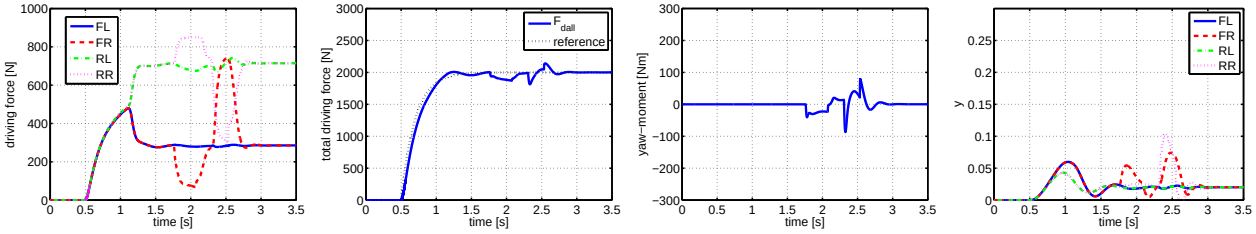

(a) $\hat{F}_d$ on each wheel. (b) $\hat{F}_{dall}$. (c) $\hat{M}_z$. (d) y on each wheel.

Fig. 16. Simulation of split slippery road (proposed).

the rear motor torque approaches to the upper limit and therefore the rear driving forces are saturated.

5.3 Split Slippery Road

Figures 15 and 16 show the simulation results of acceleration test on split slippery surface. In each result, front-right wheel is on slippery surface from about 1.8 [s] to 2.1 [s], and rear-right one is from about 2.3 [s] to 2.5 [s].

Since the traction of DFC is indicated in the previous section, result of acceleration test without control is excluded. In case with only DFC, Fig. 15(a) shows that the driving forces in only the right wheels reduce. As a result, the total driving force decreases as shown in Fig. 15(b), and the undesired yaw-moment is generated as shown in Fig. 15(c). In contrast, with the proposed method, driving force of each wheel is distributed as shown in Fig. 16(a) to retain driving force while preventing the generation of yaw-moment, which can be confirmed by comparing Fig. 15(b), 15(c) with Fig. 16(b), 16(c). In addition, compared to Fig. 15(d), Fig. 16(d) shows that the proposed method prevents the saturation of y.

6 EXPERIMENTS

6.1 Experimental Setup

In this section, experimental results on an instantaneous slippery road are explained under the same condition as the simulation in Section 5. A polymer sheet is utilized to simulate slippery road condition. This sheet, called “low-μ sheet" in this paper, can realize a friction coefficient μ of about 0.2 by watering on it. The control parameters are as same as simulation, while tuning gain of the driving force distribution is set as $\phi_r = 1.3$.

Vehicle velocity is measured using an optical sensor. Since it can not measure velocity accurately on low speed, the slip ratio of each experimental result before 1.2 [s] is not correct.

6.2 Instantaneous Slippery Road

The experimental results are shown in Fig. 17–19. Results are compared with three cases as explained in Section 5.2. In each result, front wheels are on slippery surface from about 2.0 [s] to 2.3 [s], and rear ones are on slippery surface from about 2.5 [s] to 2.7 [s].

Comparing Fig. 17(a) with Fig. 18(a) and 19(a), traction is obtained by DFC. As for driving force, without control and with only DFC, driving force decreases in Fig. 17(b), Fig. 17(c), Fig. 18(b), Fig. 18(c), similar to the simulation results. In contrast, with the proposed method, Fig. 19(b) shows that driving force on each wheel is distributed to retain total driving force as shown in Fig. 19(c). Additionally, comparing with Fig. 18(d), Fig. 19(d) shows that the proposed method prevents the saturation of y when the front wheels are on the slippery road.

Rear wheels do not reduce their driving force by the conventional method as shown in Fig. 18(b). This is be-

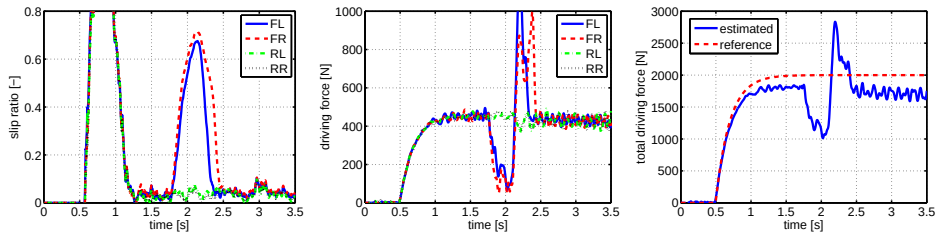

(a) λ on each wheel. (b) $\hat{F}_d$ on each wheel. (c) $\hat{F}_{dall}$.

Fig. 17. Experiment of instantaneous slippery road (without control).

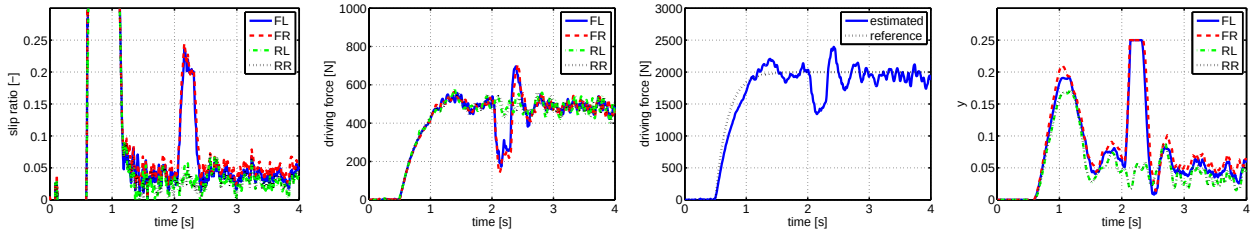

(a) λ on each wheel. (b) $\hat{F}_d$ on each wheel. (c) $\hat{F}_{dall}$. (d) y on each wheel.

Fig. 18. Experiment of instantaneous slippery road (only DFC).

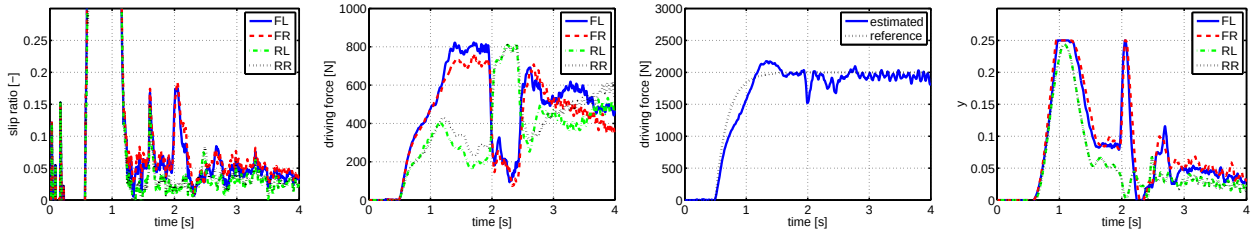

(a) λ on each wheel. (b) $\hat{F}_d$ on each wheel. (c) $\hat{F}_{dall}$. (d) y on each wheel.

Fig. 19. Experiment of instantaneous slippery road (proposed).

cause the rear static load of “FPEV2-Kanon" is larger than the front one. Moreover, load is transferred to rear axis during acceleration.

6.3 Split Slippery Road

The experimental results on the split slippery surface are shown in Fig. 20 and Fig. 21. In each result, front-right wheel is on slippery surface from about 2.0 [s] to 2.3 [s], and rear-right one is on slippery surface from about 2.5 [s] to 2.7 [s].

Similar to Section 5.3, Fig. 20 shows the results of the conventional method and Fig. 21 shows those of the proposed one. With only DFC, only the front-right driving force decreases as shown in Fig. 20(a), which leads to the diminution of the total driving force as shown in Fig. 20(b) and the generation of the undesired yaw-moment of about -200 [Nm] as shown in Fig. 20(c).

In comparison with the conventional method, the front-right and the rear-right driving force is compensated for each other as shown in Fig. 21(a), and consequently the total driving force is retained to the reference as shown in Fig. 21(b). Also the undesired yaw-moment is suppressed as shown in Fig. 21(c). Additionally, comparing with Fig. 20(d), Fig. 21(d) shows that the proposed method prevents the saturation of y.

6.4 Deceleration Test

The proposed method can also apply to deceleration as shown in Fig. 22 and Fig. 23, the results of deceleration test on instantaneous slippery surface. Vehicle accelerates to 30 [km/h] and starts to decelerate with total driving

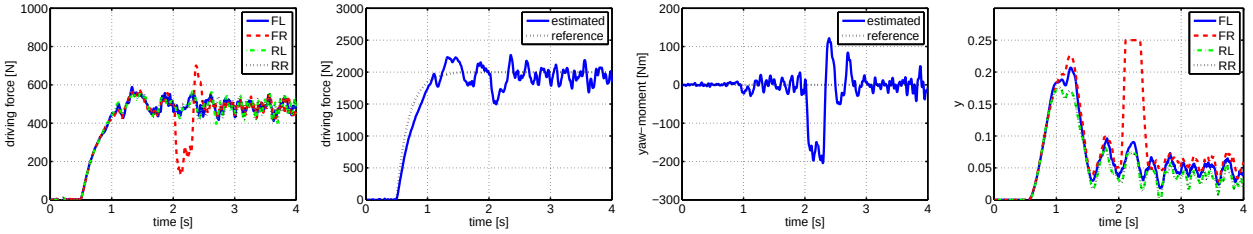

(a) $\hat{F}_d$ on each wheel. (b) $\hat{F}_{dall}$. (c) $\hat{M}_z$. (d) y on each wheel.

Fig. 20. Experiment of split slippery road (only DFC).

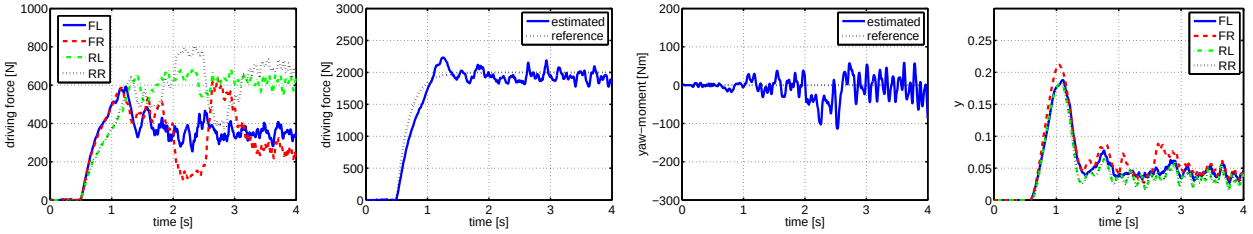

(a) $\hat{F}_d$ on each wheel. (b) $\hat{F}_{dall}$. (c) $\hat{M}_z$. (d) y on each wheel.

Fig. 21. Experiment of split slippery road (proposed).

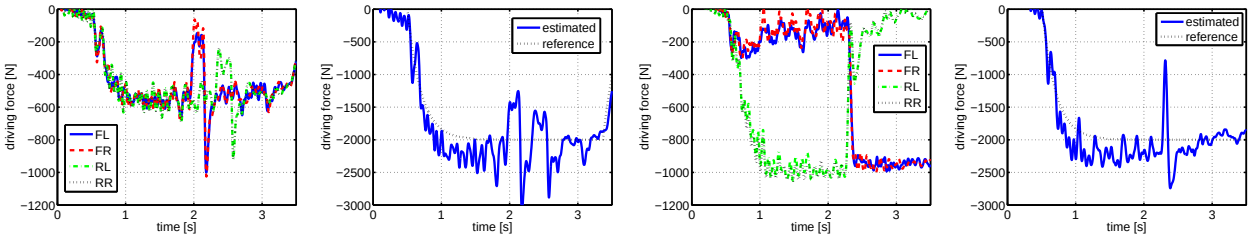

(a) $\hat{F}_d$ on each wheel. (b) $\hat{F}_{dall}$.

Fig. 22. Deceleration test (only DFC).

(a) $\hat{F}_d$ on each wheel. (b) $\hat{F}_{dall}$.

Fig. 23. Deceleration test (proposed).

force reference $F^*_{dall} = -2000$ [Nm]. The low-μ road of length 0.9 [m] is set at the distance of 8.3 [m] from the point where the vehicle starts to decelerate. In each result, front wheels are on slippery surface from about 2.0 [s] to 2.1 [s], and rear ones are on slippery surface from about 2.3 [s] to 2.5 [s].

In case with only DFC, Fig. 22(a) shows that absolute values of the front driving forces decrease on slippery surface, and next those of the rear driving forces decreases. As a result, absolute value of the total driving force decreases as shown in Fig. 22(b). On the other hand, with the proposed method, the front and rear driving forces are compensated for each other as shown in Fig. 23(a), and consequently the total driving force is retained to the reference as shown in Fig. 23(b).

7 CONCLUSION

In this paper, four-wheel driving force distribution method for instantaneous or split slippery roads is proposed, and its effectiveness is verified by simulations and experiments. With the proposed distribution method, the reduction of total driving force and generation of yaw-moment is prevented. Therefore EVs can be driven without difficulty no matter what road condition.

In future, the authors' research group plans to consider cornering and braking, to apply the estimation method of the vehicle velocity without using the optical sensor [12, 13], and to estimate λ_{peak} in realtime based on DFC.

ACKNOWLEDGMENT

This research was partly supported by the Industrial Technology Research Grant Program from the New Energy and Industrial Technology Development Organization (NEDO) of Japan (No. 05A48701d), and by the Ministry of Education, Culture, Sports, Science and Technology grant (No. 22246057).

REFERENCES

[1] Y. Hori, "Future vehicle driven by electricity and control—research on four-wheel-motored "uot electric march ii"," *IEEE Transactions on Industrial Electronics*, vol. 51, no. 5, pp. 954–962, 2004.

[2] D. Foito, M. Guerreiro, and A. Cordeiro, "Anti-slip wheel controller drive for ev using speed and torque observers," in *Proceedings of the 18th International Conference on Electrical Machines*, pp. 1–5, 2008.

[3] Y. Ge and C. S. Chang, "Torque distribution control for electric vehicle based on traction force observer," in *Proceedings of the IEEE International Conference on Computer Science and Automation Engineering*, pp. 371–375, 2011.

[4] J. Hu, D. Yin, Y. Hori, and F. Hu, "Electric vehicle traction control: A new mtte methodology," *IEEE Industry Applications Magazine*, vol. 18, no. 2, pp. 23–31, 2012.

[5] M. Kamachi, H. Miyamoto, and H. Yoshida, "Development of electric vehicle for on-road test," in *Proceedings of 9th International Symposium on Advanced Vehicle Control*, pp. 665–669, 2008.

[6] G. Zou, Y. Luo, K. Li, and X. Lian, "Slip ratio control of independent awd ev based on fuzzy dsmc," in *Proceedings of ICVES. IEEE International Conference on Vehicular Electronics and Safety 2007*, pp. 1–6, 2007.

[7] K. Xu, G. Xu, W. Li, L. Jian, and Z. Song, "Anti-skid for electric vehicles based on sliding mode control with novel structure," in *Proceedings of 2011 IEEE International Conference on Information and Automation*, pp. 650–655, 2011.

[8] E. Ono, K. Asano, M. Sugai, S. Ito, M. Yamamoto, M. Sawada, and Y. Yasui, "Estimation of automotive tire force characteristics using wheel velocity," *Control Engineering Practice*, vol. 11, no. 12, pp. 1361–1370, 2003.

[9] R. Hoseinnezhad and A. Bab-Hadiashar, "Efficient antilock braking by direct maximization of tire-road frictions," *IEEE Transactions on Industrial Electrinics*, vol. 58, no. 8, pp. 3593–3600, 2011.

[10] G. Erdogan, L. Alexander, and R. Rajamani, "Estimation of tire-road friction coefficient using a novel wireless piezoelectric tire sensor," *IEEE Sensors Journal*, vol. 11, no. 2, pp. 267–279, 2011.

[11] M. Yoshimura and H. Fujimoto, "Driving torque control method for electric vehicle with in-wheel motors," *IEEJ Transactions on Indstry Applications*, vol. 131, no. 5, pp. 1–8, 2010. (in Japanese).

[12] K. Fujii, H. Fujimoto, and N. Takahashi, "Vehicle stability control of electric vehicle with slip-ratio and cornering stiffness estimation," in *Proceedings of IEEE/ASME International Conference on Advanced Intelligent Mechatronics*, pp. 27–32, 2007.

[13] T. Suzuki and H. Fujimoto, "Slip ratio estimation and regenerative brake control without detection of vehicle velocity and acceleration for electric vehicle at urgent brake-turning," in *Proceedings of the 11th IEEE International Workshop on Advanced Motion Control*, pp. 273–278, 2010.

[14] T. Kanou and H. Fujimoto, "Slip-ratio based yaw-rate control with driving stiffness identification for electric vehicle," in *Proceedings of 9th International Symposium on Advanced Vehicle Control*, pp. 786–791, 2008.

[15] H. B. Pacejka and E. Bakker, "The magic formula tyre model," in *Tyre models for vehicle dynamic analysis: proceedings of the 1st International Colloquium on Tyre Models for Vehicle Dynamics Analysis, held in Delft, The Netherlands*, pp. 1–18, 1991.

[16] S. Sakai, *2D-Tire Model ver 1.0*. http://sakai.nnl.isas.ac.jp/index_j.html, 2000.

Kenta Maeda received the B.S. degree in Electrical Engineering from The University of Tokyo, Tokyo, Japan in 2011. He is currently a M.S. candidate in Advanced Energy at The University of Tokyo, Tokyo, Japan.
His research interests include vehicle dynamics and control in order to improve vehicle's safety and driver's comfortability for electric vehicle.
Mr. Maeda is a member of the Institute of Electrical Engineers of Japan (IEEJ), the Japan Society of Mechanical Engineers (JSME), Society of Automotive Engineers of Japan (JSAE), and the Institute of Electric and Electronics Engineers (IEEE).

Hiroshi Fujimoto received the Ph.D. degree from The University of Tokyo, Tokyo, Japan, in 2001.
In 2001, he joined the Department of Electrical Engineering, Nagaoka University of Technology, Niigata, Japan, as a Research Associate. From 2002 to 2003, he was a Visiting Scholar with the School of Mechanical Engineering, Purdue University, West Lafayette, IN. In 2004, he joined the Department of Electrical and Computer Engineering, Yokohama National University, Yokohama, Japan, as a Lecturer, and he became an Associate Professor in 2005. He has been an Associate Professor with the Department of Advanced Energy, Graduate School of Frontier Sciences, The University of Tokyo, since 2010. His research interests include control engineering, motion control, nanoscale servo systems, electric vehicle control, and motor drives.
Dr. Fujimoto is a Member of the Institute of Electrical Engineers of Japan, the Society of Instrument and Control Engineers (SICE), the Robotics Society of Japan, and the Society of Automotive Engineers of Japan. He received the Best Paper Award from the IEEE TRANSACTION ON INDUSTRIAL ELECTRONICS in 2001, the Isao Takahashi Power Electronics Award in 2010, and the Best Author Prize from the SICE in 2010.

Yoichi Hori received the B.S., M.S., and Ph.D. degrees in electrical engineering from The University of Tokyo, Tokyo, Japan, in 1978, 1980, and 1983, respectively.
In 1983, he joined the Department of Electrical Engineering, The University of Tokyo, as a Research Associate, where he later became an Assistant Professor, an Associate Professor, and, in 2000, a Professor. He moved to the Institute of Industrial Science as a Professor with the Information and System Division in 2002 and to the Department of Advanced Energy, Graduate School of Frontier Sciences, The University of Tokyo, in 2008. From 1991 to 1992, he was a Visiting Researcher with the University of California, Berkeley. His research interests are control theory and its industrial applications to motion control, mechatronics, robotics, electric vehicles, etc.
Dr. Hori has been the Treasurer of the IEEE Japan Council and Tokyo Section since 2001. He is also an Administrative Committee member of the IEEE Industrial Electronics Society and a member of the Society of Instrument and Control Engineers, the Robotics Society of Japan, the Japan Society of Mechanical Engineers, and the Society of Automotive Engineers of Japan (JSAE). He was the President of the Industry Applications Society of the Institute of Electrical Engineers of Japan (IEEJ), the President of Capacitors Forum, the Chairman of the Motor Technology Symposium of the Japan Management Association, and the Director on Technological Development of JSAE. He received the Best Transactions Paper Award from the IEEE TRANSACTION ON INDUSTRIAL ELECTRONICS in 1993 and 2001, the 2000 Best Transactions Paper Award from the IEEJ, and the 2011 Achievement Award from the IEEJ.

AUTHORS' ADDRESSES

Kenta Maeda
Prof. Hiroshi Fujimoto, Ph.D.
Prof. Yoichi Hori, Ph.D.
Department of Advanced Energy,
Graduate School of Frontier Sciences,
The University of Tokyo,
5-1-5, Kashiwanoha, Kashiwa, Chiba, 277-8561, Japan
email: maeda@hflab.k.u-tokyo.ac.jp,
fujimoto@k.u-tokyo.ac.jp, hori@k.u-tokyo.ac.jp

Received: 2012-06-30
Accepted: 2012-10-28